Yield ratios of light particles as a probe of the proton skin of a nucleus and its centrality dependence

T. Z. Yan* and S. Li
School of Energy and Power Engineering, Northeast Electric Power University, Jilin 132012, China

(Received 16 February 2020; accepted 22 April 2020; published 5 May 2020)

The yield ratios of neutron-proton [$R(n/p)$] and ^{3}H-^{3}He [$R(t/^3\mathrm{He})$] with reduced rapidity from 0 to 0.5 are simulated for 50 MeV/u ^{48,50,52,54,56,58}Ni + ^{58}Ni neutron-deficient systems at all reduced impact parameters by using the isospin-dependent quantum molecular dynamics (IQMD) model. Neutron and proton density distributions (used for the phase-space initialization of the reaction system in IQMD) and the proton skin thickness ΔR_{pn} of different neutron-deficient Ni isotopes are given by the Skyrme-Hartree-Fock model. The results show that both $R(n/p)$ and $R(t/^3\mathrm{He})$ from different centralities are strongly linear with N/Z of different Ni projectiles, but are exponentially dependent on ΔR_{pn} with better fitting. It is therefore suggested that $R(n/p)$ and $R(t/^3\mathrm{He})$ from any same centrality (peripheral collisions are much better, with bigger yield ratios and curve slopes) could be treated as possible experimental probes to extract the proton skin thickness of neutron-deficient isotopes from isotopes near the β-stability line.

DOI: 10.1103/PhysRevC.101.054601

I. INTRODUCTION

The common properties of nuclei near β-stability line are well known, including nuclear structure and nuclear reactions. The characteristics of unstable nuclei with a large excess of neutrons or protons has become one of the most important research fields of nuclear physics, and several radioactive-beam facilities have been built in the world at which many exotic nuclei far from the β-stability line have been found. Neutron-rich nuclei have been extensively studied, and the most important structural behavior of a neutron-rich nucleus is the neutron skin or halo, i.e., neutrons have much more extended density distributions than do protons. That structural property can be explored by some nuclear structure models such as the Skyrme-Hartree-Fock model [1–3], the relativistic mean-field model [4–7], the shell model [8–10], and so on. There are also some other corresponding properties due to the skin or the surface of the unstable nuclei such as small separation energy and low angular momentum of the last few nucleons, increased reaction cross section, and so on. Among the experimental probes, collective flows have been regarded as sensitive probes of isospin-dependent quantities or mechanisms, including equations of state (EOS) and especially symmetry energy, nucleon-nucleon collisions, Coulomb force, and surface properties of the colliding nuclei [11–16]. The neutron-to-proton yield ratio has also been used to explore the isospin physics, such as the symmetry energy, the in-medium nucleon-nucleon cross section, the isospin splitting of nucleon effective mass, etc. [17–23]. Neutron skin thickness is defined as the difference between the neutron and the proton root-mean-square radii, i.e., $\Delta R_{np} = \langle r^2\rangle_n^{1/2} - \langle r^2\rangle_p^{1/2}$. So the most direct way to study the skin structure is to detect the density distributions of neutrons and protons in a nucleus. Experimentally, the proton density distribution can be determined to a high accuracy by using the electron-scattering method, whereas the neutron density distribution is relatively poorly obtained by hadron-nucleus interactions due to the complex strong interactions between nucleons. Thus, the neutron skin thickness cannot be obtained with high accuracy. Although the nucleon distributions studied so far have mainly focused on stable nuclei, the nuclear charge distribution of unstable nuclei may be obtained in the near future from specially designed electron-ion colliders, e.g., the planned eA collider at the GSI Facility for Antiproton and Ion Research (FAIR) [24]. On the other hand, the use of indirect experimental observables to extract ΔR_{np} have been proposed, such as the yield ratios. Sun [25] found that the neutron-proton yield ratio $R(n/p)$ at projectile-like rapidity is strongly linear in neutron skin thickness. Later, Dai [26] proposed the yield ratio of triton to ^{3}He [$R(t/^3\mathrm{He})$] as another experimental probe of neutron skin thickness. In their work, they got different neutron and proton density distributions and ΔR_{np} for a certain Ca isotope by adjusting the diffuseness parameter in the Droplet model, and then obtained different yield ratios simulated by using an isospin-dependent quantum molecular dynamics (IQMD) model with the different neutron and proton density distributions obtained above for phase-space initialization of a Ca projectile. In the present work, we extend the yield ratio method to neutron-deficient nuclei with a proton skin thickness defined as $\Delta R_{pn} = \langle r^2\rangle_p^{1/2} - \langle r^2\rangle_n^{1/2}$. The Skyrme-Hartree-Fock method is used for different neutron-deficient Ni isotopes to obtain ΔR_{pn} and the neutron and proton density distributions, which are then used to generate the projectile initialization phase space in the IQMD model. Finally, the correlation between proton skin thicknesses and the yield ratios $R(n/p)$ and $R(t/^3\mathrm{He})$ from those neutron-deficient

*ytz0110@163.com

Ni-induced collisions ^{48,50,52,54,56,58}Ni + ^{58}Ni at 50 MeV/u are examined, and the reduced impact-parameter dependence for the above correlation are also explored.

II. THEORETICAL DESCRIPTIONS

The quantum-molecular-dynamics (QMD) approach is a successful many-body theory which well describes the state and the time evolution of the colliding system from intermediate to relativistic energies. Thus, it can provide abundant information about the reaction dynamics, the fragmentation process, and correlation effects. As a dynamical model it mainly includes the following components: the initialization of the projectile and the target nucleons, the propagation of nucleons in the effective mean field, nucleon-nucleon collisions in nuclear medium, and Pauli blocking. A general review of the QMD model can be obtained in Ref. [27], and it has been widely used in heavy-ion collisions to explore nuclear equations of state (EOS) [28–30], fragment production [31–36], collective flows [16,37–39], and even nuclear structure [25,26,40,41].

The IQMD model is based on the general QMD model affiliated with the isospin effect on the mean field, nucleon-nucleon collisions, and Pauli blocking. In the IQMD model, each nucleon is described by a Gaussian wave packet,

$$\psi_i(\vec{r},t) = \frac{1}{(2\pi L)^{3/4}} \exp\left[-\frac{[\vec{r}-\vec{r}_i(t)]^2}{4L}\right] \exp\left[-\frac{i\vec{r}\cdot\vec{p}_i(t)}{\hbar}\right], \tag{1}$$

where $\vec{r}_i(t)$ and $\vec{p}_i(t)$ are the ith wave pocket in coordinate and momentum space. L is the wave-pocket width and $L = 2.16$ fm^2 is used in the present study. All nucleons interact via the mean field and NN collisions. The nuclear mean-field potential used in the IQMD model can be parametrized as follows:

$$U(\rho,\tau_z) = \alpha\left(\frac{\rho}{\rho_0}\right) + \beta\left(\frac{\rho}{\rho_0}\right)^{\gamma} + \frac{1}{2}(1-\tau_z)V_c + C_{\rm sym}\frac{(\rho_n-\rho_p)}{\rho_0}\tau_z + U^{\rm Yuk}, \tag{2}$$

where ρ_0 is the normal nuclear matter density (0.16 fm^{-3}), ρ, ρ_p, and ρ_n are the total, proton, and neutron densities, respectively. τ_z is the zth component of the isospin degree of freedom, which equals 1 or -1 for neutrons or protons, respectively. Different coefficients α, β, and γ are used for different nuclear equations of state. $C_{\rm sym}$ is the symmetry energy strength due to the asymmetry of neutrons and protons in a nucleus. In this study, we adopt $\alpha = -356$ MeV, $\beta = 303$ MeV, and $\gamma = 1.17$ which corresponds to the so-called soft EOS with an incompressibility of $K = 200$ MeV and $C_{\rm sym} = 32$ MeV, because the soft EOS describes relatively well the yields of fragments in previous studies. V_c is the Coulomb potential and $U_{\rm Yuk}$ is the Yukawa (surface) potential.

In the IQMD model, fragments emitted in a reaction are commonly identified by coalescence mechanism, in which nucleons with relative spatial distance Δr smaller than 3.5 fm and relative momentum difference Δp smaller than 300 MeV/c will be recognized as a part of a fragment [27].

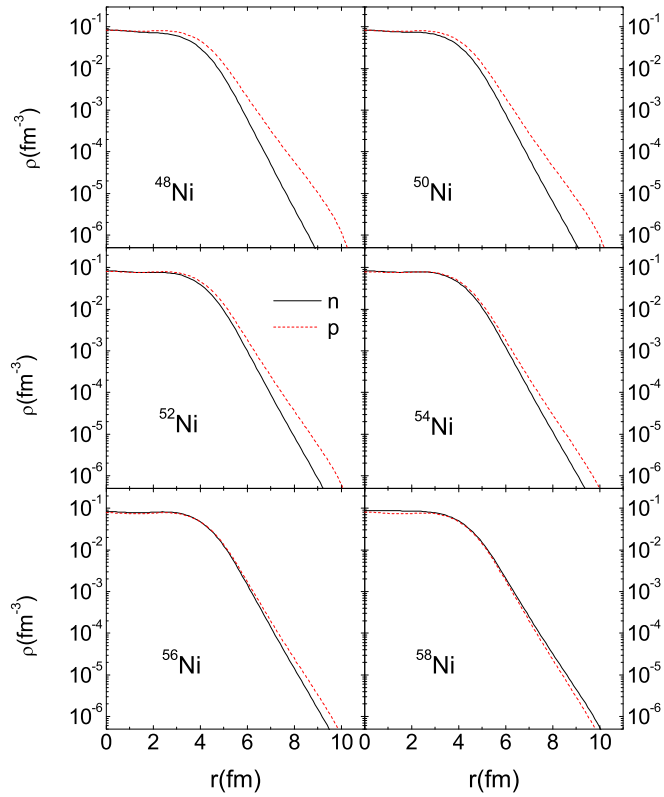

FIG. 1. Normalized neutron (solid lines) and proton (dashed lines) density distributions of ^{48,50,52,54,56,58}Ni calculated with the SkM* parametrization of the SHF method.

The nucleon-nucleon cross section used in the model is the experimental parametrization, which is also isospin dependent. The cross section between neutron and proton is about three times larger than that between proton and proton or neutron and neutron when reaction energy is below 300 MeV/u.

III. RESULTS AND DISCUSSION

IQMD can better describe medium and heavy rather than light ion reactions, while proton skin structure is more likely to be formed in relatively light nuclei, so the element Ni, which has a relatively large number of proton-rich isotopes, is selected in this work. The phase-space initialization of the projectile and target for IQMD is based on the neutron and proton density distributions of the projectile and target nuclei extracted by Skyrme-Hartree-Fock (SHF) theory with the so-called SkM* parametrization, from which the calculated ΔR_{pn} of ^{48,50,52,54,56,58}Ni isotopes are 0.284, 0.211, 0.151, 0.1, 0.056, and 0.002 fm, respectively. The normalized neutron and the proton density distributions of ^{48,50,52,54,56,58}Ni are shown in Fig. 1. It can be observed that, with decreasing neutron number in Ni neutron-deficient isotopes, the difference between neutron and proton density distributions at the edge of the Ni nucleus becomes more and more distinct, and there is clearly a proton skin structure in ^{48,50,52}Ni. These calculated ΔR_{np} are nearly equal to the corresponding results in Ref. [42] using the deformed self-consistent mean-field Skyrme HF + BCS method with SLy4 parametrization, which

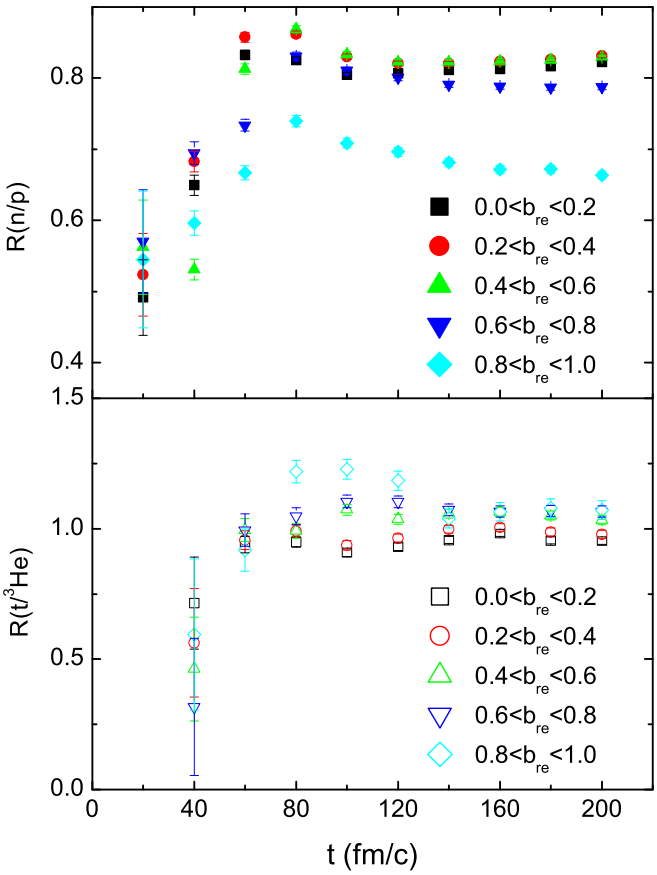

FIG. 2. Time evolution of the yield ratios $R(n/p)$ (solid symbols) and $R(t/^3\mathrm{He})$ (open symbols) with $0 < y < 0.5$ and from $^{52}\mathrm{Ni} + ^{58}\mathrm{Ni}$ at 50 MeV/u. Different symbol types represent ratios from different centrality collisions.

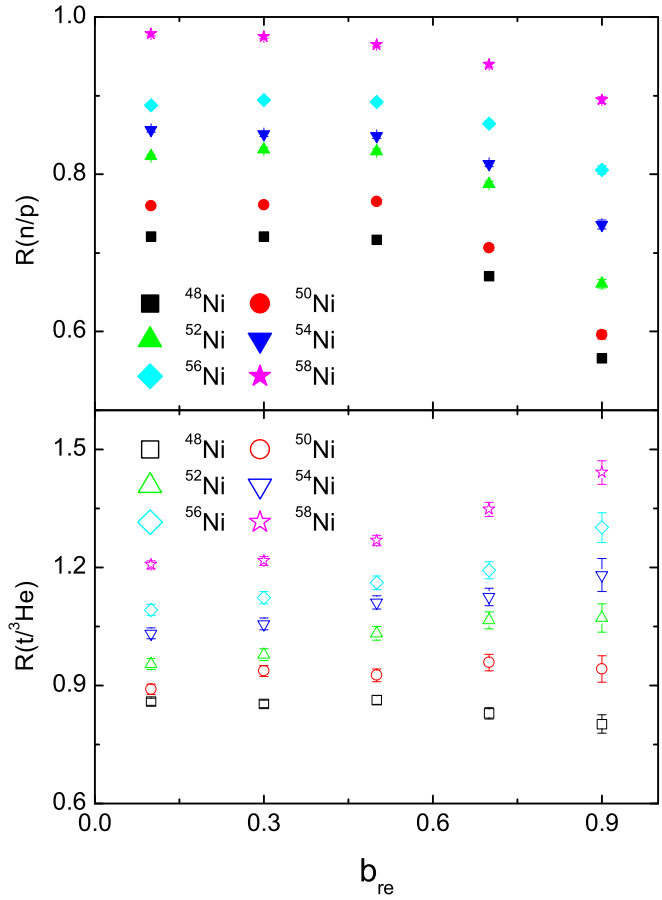

FIG. 3. The reduced impact-parameter dependence of the yield ratios of $R(n/p)$ (solid symbols) and $R(t/^3\mathrm{He})$ (open symbols) with $0 < y < 0.5$ from $^{48,50,52,54,56,58}\mathrm{Ni} + ^{58}\mathrm{Ni}$ at 50 MeV/u. Different symbol types represent the ratios from collisions induced by different projectiles.

we extract roughly from its figure as 0.26, 0.20, 0.14, 0.09, 0.05, and 0.005 fm, respectively. In addition, the calculated ΔR_{np} of ^{58}Ni falls within the experimental limit of $-0.09^{+0.09}_{-0.16}$ fm [43].

The total centrality of collisions of $^{48,50,52,54,56,58}\mathrm{Ni} + ^{58}\mathrm{Ni}$ at 50 MeV/u are simulated by the IQMD model with the soft EOS. The reduced impact parameter is used to describe the centrality of the collision as $b_{re} = b/b_{\max}$ where $b_{\max}$ is the total of the radii of projectile and target nuclei. In this paper, the physical results of the fragments are calculated in the center-of-mass frame and limited to projectile-like midrapidity, i.e., the reduced rapidity in the center-of-mass frame [$y = (y/y_p)_{\mathrm{c.m.}}$, where y_p is the rapidity of the projectile between 0 and 0.5]. The yield ratios $R(n/p)$ and $R(t/^3\mathrm{He})$ can be calculated with the yields of neutrons, protons, ^{3}H, and ^{3}He.

The time evolution of the yield ratios of $R(n/p)$ and $R(t/^3\mathrm{He})$ from $^{52}\mathrm{Ni} + ^{58}\mathrm{Ni}$ as an example are investigated as shown in the upper and lower panels of Fig. 2, respectively. It is seen that the yield ratios of $R(n/p)$ and $R(t/^3\mathrm{He})$ from midrapidity in all centralities are stable after 140 fm/c. To improve statistics, we accumulate the studied fragments from 160 to 200 fm/c.

Figure 3 compares the reduced-impact-parameter dependence for different Ni isotopes. It is seen that the yield ratios $R(n/p)$ and $R(t/^3\mathrm{He})$ from Ni isotopes with bigger constituent N/Z-induced reactions are larger at the same reduced impact parameter, which is apparently reasonable that fragments at $0 < y < 0.5$ are from the projectile. It also shows that the yield ratios $R(n/p)$ descend with the reduced impact parameter, which may be due to the greater influence of the proton skin at bigger collision parameters, while the ratios $R(t/^3\mathrm{He})$ increase with b_{re}, especially for heavier Ni isotopes with higher N/Z, and $R(t/^3\mathrm{He})$ is larger than $R(n/p)$ for a certain projectile, which may mean that the fragments emitted from the overlapping area prefer more neutrons than protons due to Coulomb repulsion. And on average, $R(t/^3\mathrm{He})$ is bigger while $R(n/p)$ is smaller than the projectile's N/Z, which is in accordance with the experimental result [20]. In other words, the yield ratios from projectile-like midrapidities should reflect the characteristics of the nucleon composition of the projectile. To explore the relation between yield ratios and projectile N/Z, Fig. 4 is plotted for different centralities. There is a clear linear positive correlation between $R(n/p)$, $R(t/^3\mathrm{He})$, and N/Z for all centralities, and the more peripheral

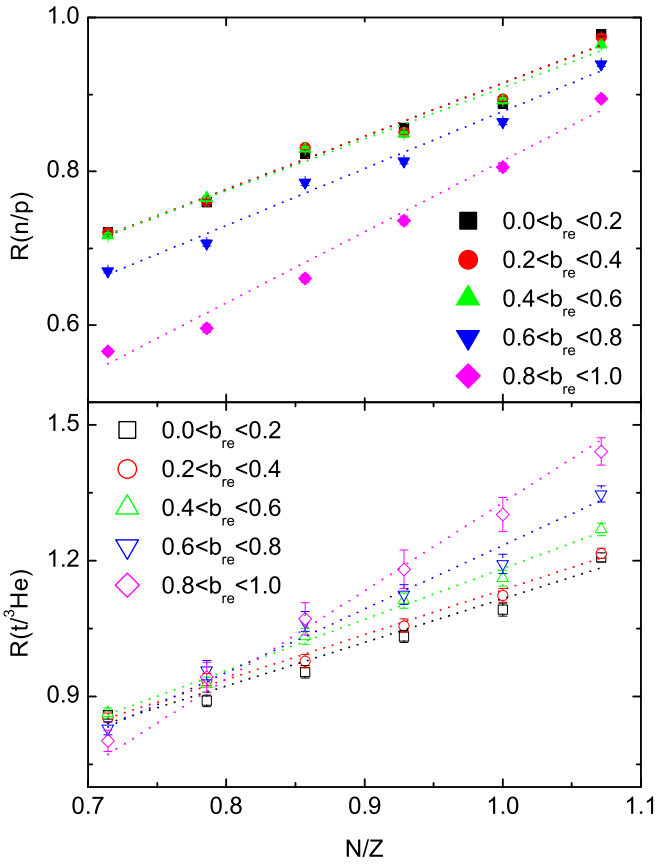

FIG. 4. The projectile's N/Z dependence of the yield ratios of $R(n/p)$ (solid symbols) and $R(t/^3\mathrm{He})$ (open symbols) with $0 < y < 0.5$ from $^{48,50,52,54,56,58}\mathrm{Ni} + ^{58}\mathrm{Ni}$ at 50 MeV/u. Different symbol types represent the ratios from different centrality collisions. The dotted lines are linear fits.

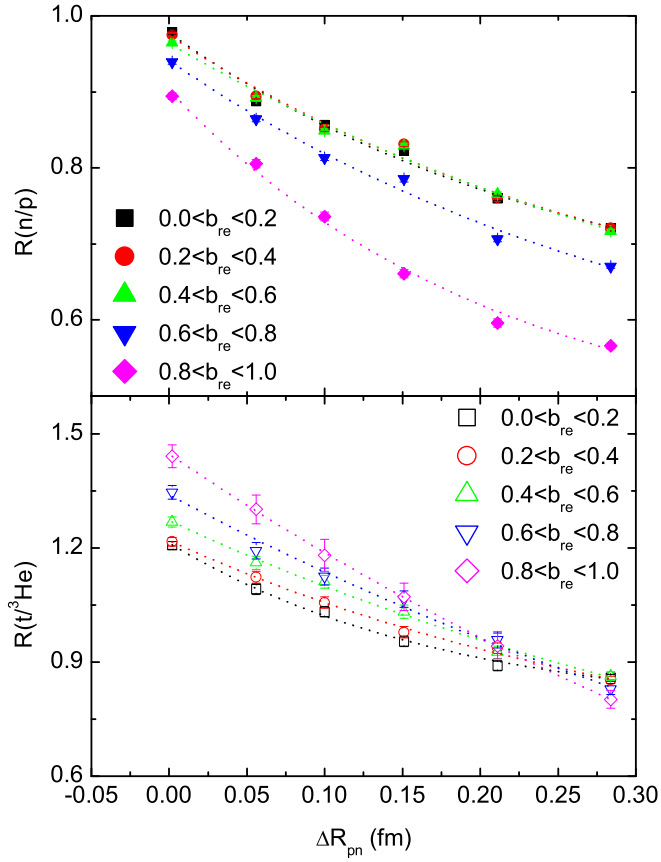

FIG. 5. Similar to Fig. 4 but for ΔR_{pn} dependence. The dotted lines are exponential fits.

the collision is, the bigger the slope is. This may indicate that the main reaction mechanism is the same at the same b_{re} for the collisions induced by different projectiles.

From the above discussion we know that the proton skin can affect the yield ratios, so the proton-skin-thickness dependence of the yield ratios is displayed in Fig. 5. It shows that the yield ratios from different centralities both decrease with proton skin thickness ΔR_{pn}, in other words, the yield ratios from a Ni projectile with thicker proton skin (i.e., smaller N/Z) are smaller, and the yield ratios descend more rapidly for peripheral reactions, which is consistent with Fig. 4. It may be understood as follows: The projectile-like fragments are emitted mainly from the projectile part of the overlap zone, so the yield ratios are close to the projectile's N/Z; meanwhile the projectile with a thicker proton skin has fewer neutrons for neutron-deficient Ni isotopes, so the yield ratios from projectiles with a thicker proton skin should be smaller. Every curve from different centralities looks like a straight line (similar to the work of Sun and Dai [25,26]), but a better R squared ($R^2 > 0.985$) can be obtained if an exponential function [$y = a\exp(-x/b) + c$] is used to fit the points. This means that the yield ratios of $R(n/p)$ or $R(t/^3\mathrm{He})$ from all the different neutron-deficient isotopic projectiles at the same reduced impact parameter attenuates in the minus exponential rule according to their proton skin thickness. So we can deduce an isotope's proton skin thickness from the other known neutron-deficient isotopes through the detection of the midrapidity yield ratios of $R(n/p)$ or $R(t/^3\mathrm{He})$ emitted from the collisions induced by these isotopes, especially peripheral reactions in which there is a stronger trend between the yield ratios and ΔR_{pn}.

The dependence of the double ratios $R(t/^3\mathrm{He})/R(n/p)$ on the proton skin thickness of $^{48,50,52,54,56,58}\mathrm{Ni}$ is shown in Fig. 6. It seems that, upon increasing ΔR_{np}, the double ratio from neutron-deficient projectiles of Ni isotopes is almost constant for different centralities, and the double ratio is bigger for peripheral collisions, which may be because the yields of the relatively heavy particles triton and ^{3}He are higher due to less energy being deposited in the overlap zone in peripheral reactions. This means that $R(t/^3\mathrm{He})$ is almost proportional to $R(n/p)$ at whole centralities, so both $R(n/p)$ and $R(t/^3\mathrm{He})$ could be regarded as experimental probes to determine proton skin thickness, especially $R(t/^3\mathrm{He})$ because charged particles are easier to measure than neutrons in the experiment.

IV. SUMMARY

The yield ratios of projectile-like particles neutron to proton and ^{3}H to ^{3}He are extracted from $^{48,50,52,54,56,58}\mathrm{Ni} + ^{58}\mathrm{Ni}$

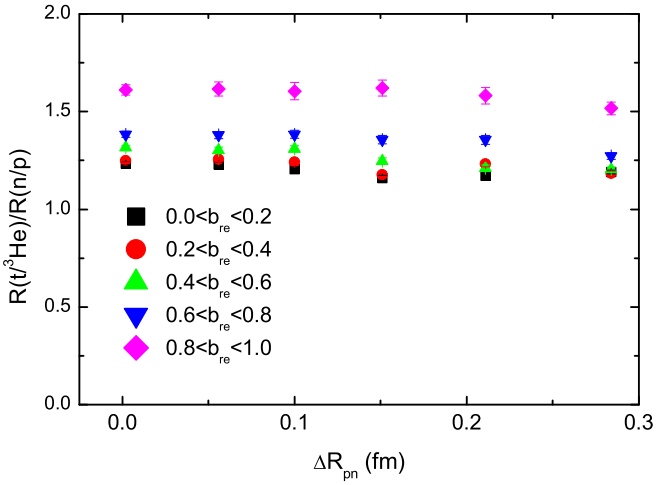

FIG. 6. Double ratio $R(t/^3\mathrm{He})/R(n/p)$ with $0 < y < 0.5$ as a function of ΔR_{np} from $^{48,50,52,54,56,58}\mathrm{Ni} + ^{58}\mathrm{Ni}$ at 50 MeV/u. Different symbol types represent the ratios from different centrality collisions.

collisions at 50 MeV/u, which are simulated by the IQMD model with the initial nucleon densities sampled by using the Skyrme-Hartree-Fock method. It is found that these ratios from the same centrality are linearly dependent on the projectile's neutron-proton ratio and exponentially dependent on the proton skin thickness ΔR_{pn} of the neutron-deficient Ni projectiles, and bigger ratios and larger slopes of the above correlation curves are gained in more peripheral reactions. Thus, we can use $R(n/p)$ and $R(t/^3\mathrm{He})$ as experimental observables to probe the proton skin thickness of neutron-deficient nuclei, i.e., we can deduce ΔR_{pn} of a neutron-deficient nucleus, especially near the proton drip line, through the exploration of $R(n/p)$ or $R(t/^3\mathrm{He})$ from other isotopic nuclei near the β-stable line. Based on the above proton skin thickness, one can try to constrain the symmetry energy in a theoretical framework and get more information about symmetry energy.

ACKNOWLEDGMENT

This work was supported by the National Natural Science Foundation of China under Grant No. 11405025.

[1] C. J. Horowitz, S. J. Pollock, P. A. Souder, and R. Michaels, Phys. Rev. C **63**, 025501 (2001).
[2] P. Danielewicz, Nucl. Phys. A **727**, 233 (2005).
[3] M. Liu, N. Wang, Z. X. Li *et al.*, Chin. Phys. Lett. **23**, 804 (2006).
[4] Z. J. Wang and Z. Z. Ren, Phys. Rev. C **70**, 034303 (2004).
[5] S. Yoshida and H. Sagawa, Phys. Rev. C **69**, 024318 (2004).
[6] A. Bhagwat and Y. K. Gambhir, Phys. Rev. C **73**, 054601 (2006).
[7] J. G. Chen, X. Z. Cai, H. Y. Zhang *et al.*, Chin. Phys. Lett. **20**, 1021 (2003).
[8] K. Bennaceur, F. Nowacki, J. Okolowicz *et al.*, Nucl. Phys. A **651**, 289 (1999).
[9] K. Kaneko, Y. Sun, and G. Angelis, Nucl. Phys. A **957**, 144 (2017).
[10] Z. H. Sun, Q. Wu, Z. H. Zhao *et al.*, Phys. Lett. B **769**, 227 (2017).
[11] B. A. Li and C. M. Ko, Nucl. Phys. A **654**, 797c (1999).
[12] L. W. Chen, F. S. Zhang, and Z. Y. Zhu, Phys. Rev. C **61**, 067601 (2000).
[13] V. N. Russkikh and Y. B. Ivanov, Phys. Rev. C **74**, 034904 (2006).
[14] Z. Q. Feng, Nucl. Phys. A **919**, 32 (2013).
[15] H. Y. Zhang, W. Q. Shen, Y. G. Ma *et al.*, Eur. Phys. J. A **15**, 399 (2002).
[16] S. Gautam, A. D. Sood, R. K. Puri, and J. Aichelin, Phys. Rev. C **83**, 014603 (2011).
[17] J. Y. Liu, Q. Zhao, S. J. Wang *et al.*, Nucl. Phys. A **687**, 475 (2001).
[18] X. C. Zhang, B. A. Li, L. W. Chen *et al.*, Chin. Phys. Lett. **26**, 052502 (2009).
[19] H. L. Liu, G. C. Yong, and D. H. Wen, Phys. Rev. C **91**, 024604 (2015).
[20] D. Thériault, J. Gauthier, F. Grenier *et al.*, Phys. Rev. C **74**, 051602(R) (2006).
[21] Y. X. Zhang, M. B. Tsang, Z. X. Li *et al.*, Phys. Lett. B **732**, 186 (2014).
[22] W.-J. Xie, J. Su, L. Zhu, and F.-S. Zhang, Phys. Rev. C **88**, 061601(R) (2013).
[23] J. Su, L. Zhu, C.-Y. Huang, W.-J. Xie, and F.-S. Zhang, Phys. Rev. C **94**, 034619 (2016).
[24] A. N. Antonov, M. K. Gaidarov, M. V. Ivanov *et al.*, Nucl. Instrum. Methods Phys. Res., Sect. A **637**, 60 (2011).
[25] X. Y. Sun, D. Q. Fang, Y. G. Ma *et al.*, Phys. Lett. B **682**, 396 (2010).
[26] Z. T. Dai, D. Q. Fang, Y. G. Ma, X. G. Cao, and G. Q. Zhang, Phys. Rev. C **89**, 014613 (2014).
[27] J. Aichelin, Phys. Rep. **202**, 233 (1991).
[28] M. B. Tsang, Y. Zhang, P. Danielewicz, M. Famiano, Z. Li, W. G. Lynch, and A. W. Steiner, Phys. Rev. Lett. **102**, 122701 (2009).
[29] Z. Q. Feng and G. M. Jin, Phys. Lett. B **683**, 140 (2010).
[30] Q. Li, Z. Li, S. Soff, M. Bleicher, and H. Stöcker, Phys. Rev. C **72**, 034613 (2005).
[31] Y. G. Ma, W. Q. Shen, and Z. Y. Zhu, Phys. Rev. C **51**, 1029 (1995).
[32] F.-S. Zhang, L.-W. Chen, Z.-Y. Ming, and Z.-Y. Zhu, Phys. Rev. C **60**, 064604 (1999).
[33] V. S. Uma Maheswari, C. Fuchs, A. Faessler, Z. S. Wang, and D. S. Kosov, Phys. Rev. C **57**, 922 (1998).
[34] S. Kumar, S. Kumar, and R. K. Puri, Phys. Rev. C **81**, 014611 (2010).
[35] N. Wang, X. Wu, and Z. Li, Phys. Rev. C **67**, 024604 (2003).
[36] Y. Zhang, Z. Li, C. Zhou, and M. B. Tsang, Phys. Rev. C **85**, 051602(R) (2012).
[37] C. Liewen, Z. Fengshou, and J. Genming, Phys. Rev. C **58**, 2283 (1998).
[38] R. Bansal, S. Gautam, R. K. Puri, and J. Aichelin, Phys. Rev. C **87**, 061602(R) (2013).
[39] FOPI Collaboration, Nucl. Phys. A **876**, 1 (2012).

[40] X. G. Cao, X. Z. Cai, Y. G. Ma, D. Q. Fang, G. Q. Zhang, W. Guo, J. G. Chen, and J. S. Wang, Phys. Rev. C **86**, 044620 (2012).

[41] J. Y. Liu, W. J. Guo, Z. Z. Ren *et al.*, Phys. Lett. B **617**, 24 (2005).

[42] P. Sarriguren, M. K. Gaidarov, E. M. de Guerra, and A. N. Antonov, Phys. Rev. C **76**, 044322 (2007).

[43] J. Jastrzbski, A. Trzcińska, P. Lubiński *et al.*, Int. J. Mod. Phys. E **13**, 343 (2004).